# Microscopic calculation and local approximation of the spatial dependence of the pairing field with bare and induced interactions

A. Pastore,[1,2] F. Barranco,[3] R. A. Broglia,[1,2,4] and E. Vigezzi[2]
[1]*Dipartimento di Fisica, Università degli Studi di Milano, via Celoria 16, I-20133 Milano, Italy*
[2]*INFN, Sezione di Milano, via Celoria 16, I-20133 Milano, Italy*
[3]*Departamento de Fisica Aplicada III, Escuela Superior de Ingenieros, Camino de los Descubrimientos s/n, E-41092 Sevilla, Spain*
[4]*The Niels Bohr Institute, University of Copenhagen, Blegdamsvej 17, DK-2100 Copenhagen Ø, Denmark*
(Received 6 December 2007; revised manuscript received 4 June 2008; published 28 August 2008)

The bare nucleon-nucleon interaction is essential for the production of pair correlations in nuclei, but an important contribution also arises from the induced interaction resulting from the exchange of collective vibrations between nucleons moving in time reversal states close to the Fermi energy. The pairing field resulting from the summed interaction is strongly peaked at the nuclear surface. It is possible to reproduce the detailed spatial dependence of this field by using either a local approximation, which fully takes into account finite size effects, or a contact interaction, with parameters that are quite different from those commonly used in more phenomenological approaches.

DOI: 10.1103/PhysRevC.78.024315 PACS number(s): 21.10.−k, 21.30.Fe, 21.60.Jz

## I. INTRODUCTION

Pairing correlations influence the basic properties of atomic nuclei in an essential way [1]. A consistent approach for describing these correlations employs a bare nucleon-nucleon interaction whose parameters are fitted to reproduce the experimental phase shifts (such as the $v_{14}$ Argonne potential) and includes medium polarization effects. The exchange of vibrations between nucleons moving in time reversal states lying close to the Fermi energy has been shown to account in both stable and halo nuclei for a consistent fraction of the pairing gap and of the two-nucleon separation energy [2–8]. The coupling of nucleons and vibrations renormalizes in an important way the single-particle properties of atomic nuclei, leading to changes in the level densities at the Fermi energy and to a breaking of single-particle strength (dynamical shell model [9]). As a rule, the dynamical shell model phenomena are simply parametrized in terms of an effective mass and spectroscopic factors. In this paper we follow the rule and concentrate on the detailed study of the spatial dependence of the pairing field, without pretending to achieve a precise estimate of the values of the pairing gap and of the condensation energy. We plan to return to the issue in a future publication, taking the variety of medium polarization effects into account in a self-consistent and unified way within the framework of the approach employed in Ref. [2], based on the solution of the Nambu-Gorkov equations and using renormalized quasiparticle random phase approximation phonons to describe the collective modes.

The main subject of the present work is the spatial dependence of the neutron pairing field and pairing density in $^{120}$Sn associated with the bare and induced pairing interaction.

In atomic nuclei, the coherence length is a few times larger than the nuclear radius. Consequently, a simple local density approximation, based on the results obtained in uniform matter, is not expected to lead to accurate results in the case of the finite system. The fact that the wave function of the Cooper pair is largely independent of the nuclear interaction, being dominated by the spatial dependence of a few orbitals lying around the Fermi surface, testifies to this expectation. We shall instead parametrize our results in terms of a local approximation that reproduces the spatial dependence of the pairing field resulting from the microscopic calculations. In this way, the presence of the nuclear surface is taken into account in an effective way. This will allow us to make a detailed comparison with effective forces commonly used to calculate pairing correlations, such as the Gogny force and zero-range, density-dependent interactions.

## II. SOLUTION OF HFB EQUATIONS AND THE SPATIAL DEPENDENCE OF THE PAIRING FIELD

We start by performing a Hartree-Fock (HF) calculation with the two-body interaction SLy4 [10] (associated with a $k$-mass $m_k \simeq 0.7m$ at saturation density), obtaining a set of single-particle energy levels $e_{nlj}$. Using different pairing interactions, which will be discussed in the following, we then solve in the calculated HF basis the Hartree-Fock-Bogoliubov (HFB) equations in the pairing channel,

$$\begin{aligned}(e_{nlj} - e_F)U^q_{nlj} + \sum_{n'} \Delta_{nn'lj} V^q_{n'lj} &= E^q_{lj} U^q_{nlj},\\ \sum_{n'} \Delta_{nn'lj} U^q_{n'lj} - (e_{nlj} - e_F)V^q_{nlj} &= E^q_{lj} V^q_{nlj},\end{aligned} \tag{1}$$

where $E^q_{lj}$ denotes the quasiparticle energy, $U^q_{nlj}$ and $V^q_{nlj}$ are the associated amplitudes, $e_{nlj}$ denote the HF single-particle energies, and $e_F$ is the Fermi energy. The calculation are performed in a spherical box of radius $R_{\rm box} = 15$ fm. From the quasiparticle amplitudes one can construct the abnormal density, also referred to as the Cooper pair wave function:

$$\Phi(\vec{r}_1, \vec{r}_2) = \sum_{qnn'lj} \frac{2j+1}{2} U^q_{nlj} V^q_{n'lj} \psi_{nn'lj}(\vec{r}_1, \vec{r}_2), \tag{2}$$

 

where $\psi_{nn'lj}(\vec{r}_1,\vec{r}_2) = [\phi_{nlj}(\vec{r}_1)\phi_{n'lj}(\vec{r}_2)]_{00}$ is the wave function of two neutrons coupled to $J=0$. We shall only consider the $S=0$ component of $\Phi$, $\Phi^{S=0}$, which is by far the dominant one. We then insert in Eq. (2), in place of $\psi_{nn'lj}$, the function

$$\psi^{S=0}_{nn'lj}(\vec{r}_1,\vec{r}_2) = \langle \vec{r}_1,\vec{r}_2|nn'lj;J=0\rangle_{S=0} = \frac{1}{4\pi}\varphi_{nlj}(r_1)/r_1\varphi_{n'lj}(r_2)/r_2 P_l(\cos\theta_{12}), \quad (3)$$

where $P_l$ is a Legendre polynomial.

The matrix elements of the pairing field are obtained self-consistently from the abnormal density by using the state-dependent gap

$$\Delta_{nn'lj} = -\langle nn'lj;J=0|v|\Phi\rangle, \quad (4)$$

where $v$ is the pairing interaction.

In the present paper we shall determine the spatial dependence of the pairing gap, using a simplified version of the formalism adopted in Ref. [2], which is convenient to make contact with phenomenological approaches (cf. the discussion in the Appendix of Ref. [7]). The total interaction is given by the sum of the bare nucleon-nucleon interaction, here taken to be the Argonne $v_{14}$ interaction $v_{\rm Arg}$, and of the interaction induced by the exchange of vibrations, $v_{\rm ind}$. We shall renormalize the matrix elements $v_{\rm Arg}+v_{\rm ind}$ of the total interaction, using matrix elements $v_{\rm Arg+ind}$ that take into account fragmentation and self-energy effects:

$$\langle \nu_1' m' \nu_2' \bar{m}'|v_{\rm Arg+ind}|\nu_1 m \nu_2 \bar{m}\rangle = Z\langle \nu_1' m' \nu_2' \bar{m}'|v_{\rm Arg}+v_{\rm ind}|\nu_1 m \nu_2 \bar{m}\rangle, \quad (5)$$

where $\nu$ stands for $\{nlj\}$, $|\bar{m}\rangle$ denotes the time reversed state, $|\bar{m}\rangle = (-1)^{m+j}|-m\rangle$, and $Z$ denotes an average value of the quasiparticle strength at the Fermi energy. In the following we shall use the typical value $Z=0.7$ [4,9]. Vertex corrections are not considered, because their contribution to the pairing gap has been found to be very small in the detailed calculation performed by solving the Nambu-Gorkov equation [2].

The matrix elements of the interaction induced by the exchange of a vibration will be calculated by evaluating the diagrams shown in Fig. 1, using the same formalism already employed in Ref. [5]:

$$\langle \nu_1' m' \nu_2' \bar{m}'|v_{\rm ind}|\nu_1 m \nu_2 \bar{m}\rangle = \sum_{J^\pi Mi}\frac{(f+g)^{\nu_1' m'}_{\nu_1 m;J^\pi Mi}(f-g)^{\nu_2' m'}_{\nu_2 m;J^\pi Mi}}{E_0-(|e_{\nu_1'}-e_F|+|e_{\nu_2}-e_F|+\hbar\omega_{J^\pi i})} + \sum_{J^\pi Mi}\frac{(f+g)^{\nu_1' m'}_{\nu_1 m;J^\pi Mi}(f-g)^{\nu_2' m'}_{\nu_2 m;J^\pi Mi}}{E_0-(|e_{\nu_1}-e_F|+|e_{\nu_2'}-e_F|+\hbar\omega_{J^\pi i})}. \quad (6)$$

The index $i$ labels the exchanged vibrational modes, having a given angular momentum and parity $J^\pi M$ and an energy $\hbar\omega_{J^\pi i}$. The modes have been calculated in the quasiparticle random phase approximation (QRPA), by using the same SLy4 interaction already employed to calculate the mean field, with the exception of the spin-orbit and Coulomb parts [11]. $E_0$ is the pairing correlation energy of a Cooper pair, a quantity that is of the order of $-2\Delta_F$, where $\Delta_F$ is the average value of the gap close to the Fermi energy. In Eq. (6) $f$ and $g$ denote the particle-vibration coupling vertices associated with the spin-independent and spin-dependent parts of the residual interaction, respectively,

$$v_{\rm ph}(\vec{r},\vec{r}') = \delta(\vec{r}-\vec{r}')\{[F_0(r)+F_0'(r)\vec{\tau}\cdot\vec{\tau}'] + [(G_0(r)+G_0'(r)\vec{\tau}\cdot\vec{\tau}')\vec{\sigma}\cdot\vec{\sigma}']\}. \quad (7)$$

In the calculation of the particle-vibration coupling we neglected the momentum-dependent part of the interaction (this part is instead taken into account in the QRPA calculation). The vertex $f$ is given by

$$f^{\nu' m'}_{\nu m;J^\pi Mi} = i^{l-l'}\langle j'm'|(i)^J Y_{JM}|jm\rangle\int dr\varphi_{\nu'}[(F_0+F_0')\delta\rho^i_{J^\pi n} + (F_0-F_0')\delta\rho^i_{J^\pi p}]\varphi_\nu, \quad (8)$$

where $F_0$, $F_0'$ are the generalized Landau-Migdal parameters associated with the SLy4 force and controlling the isoscalar and isovector spin-independent channels and $\delta\rho^i_{J^\pi n}$ and $\delta\rho^i_{J^\pi p}$ are, respectively, the neutron and proton contributions to the transition densities and are given by

$$\delta\rho^i_{J^\pi}(r) = \frac{1}{\sqrt{2J+1}}\sum_{\nu_1,\nu_2}[X_{\nu_1,\nu_2}(i,J^\pi)+Y_{\nu_1,\nu_2}(i,J^\pi)] \times\left(u_{\nu_1}v_{\nu_2}+u_{\nu_2}v_{\nu_1}\right)\langle\nu_1||i^J Y_J||\nu_2\rangle\varphi_{\nu_1}(r)/r\varphi_{\nu_2}(r)/r. \quad (9)$$

The vertex $g$ is given by

$$g^{\nu' m'}_{\nu m J^\pi Mi} = \sum_{L=J-1}^{J+1} i^{l-l'}\langle j'm'|(i)^L[Y_L\times\sigma]_{JM}|jm\rangle \quad (10)$$

$$\int dr\varphi_{\nu'}[(G_0+G_0')\delta\rho^i_{J^\pi Ln}+(G_0-G_0')\delta\rho^i_{J^\pi Lp}]\varphi_\nu, \quad (11)$$

where $G_0$, $G_0'$ are the generalized Landau-Migdal parameters controlling the isoscalar and isovector spin-dependent channels and $\delta\rho^i_{J^\pi Ln}$ and $\delta\rho^i_{J^\pi Lp}$ are, respectively, the neutron and

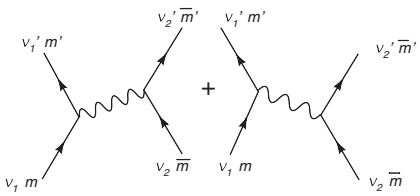


FIG. 1. Diagrams showing the exchange of a vibration between two pairs of levels coupled to $J=0$.

proton contributions to the transition densities and are given by

$$\delta\rho^{i}_{J^\pi L}(r) = \frac{1}{\sqrt{2J+1}} \sum_{\nu_1,\nu_2} [X_{\nu_1,\nu_2}(i, J^\pi) - Y_{\nu_1,\nu_2}(i, J^\pi)] \times \left(u_{\nu_1} v_{\nu_2} + u_{\nu_2} v_{\nu_1}\right) \times \langle \nu_1 || i^L [Y_L \times \sigma]_J || \nu_2 \rangle \times \varphi_{\nu_1}(r)/r \varphi_{\nu_2}(r)/r. \quad (12)$$

The values of the Landau-Migdal parameters associated with the SLy4 interaction are shown in Fig. 2. We observe that only the vertices $g$, associated with the spin-dependent part of the residual interaction, can contribute in the case of non-natural parity phonons (for which $J = L + 1$ or $J = L - 1$), whereas both $f$ and $g$ can contribute in the case of natural-parity phonons (for which $J = L$). We have included phonons of both parities having energy up to 30 MeV, associated with multipolarities from $J = 0$ to $J = 5$. We have verified that the results are essentially the same including multipolarities up to $J = 8$. This is in keeping with the fact that low-lying vibrations tend to lose their collective character, when the associated wavelength becomes of the order of the interparticle distance or smaller than it [1]. The calculation of the matrix elements of the induced interaction is then the same as performed in Ref. [5], except for the fact that there the SkM* interaction was used, instead of the SLy4 one (with the influence of $0^+$, $0^-$, and $1^-$ multipolarities, which were not included in Ref. [5], being negligible). The main difference between the two interactions lies in the value of the effective mass, which is higher in the SkM* case, corresponding to a higher level density close to the Fermi energy and therefore leading to larger pairing gaps.

We remark that only the results obtained by making use of the total interaction $v_{\text{Arg+ind}}$ have physical meaning and should be compared with experiment. However, to better understand the properties of the total interaction and to make contact with the literature we shall also study the Argonne and the induced interactions separately. It is important to notice that *in these two cases the matrix elements will not be multiplied by Z*.

The diagonal matrix elements $\Delta_{nnlj}$ of the state-dependent pairing gap obtained by solving the HFB equations with the matrix elements $v_{\text{Arg+ind}}$ [cf. Eq. (5)] are shown in Fig. 3 (squares). We plot the results for single-particle states with energy less than 100 MeV but we note that to reach convergence within 100 keV for the pairing gap, due to the presence of a strong repulsive core in the Argonne interaction, we have to include single-particle levels with energy up to 800 MeV in the HFB equations. For clarity, here and in following figures, the matrix elements for $e_{nlj} > 0$ have been averaged over intervals of 3 MeV in width. For large values of $e_{nlj}$, they assume small negative values, again due to the presence of the strong repulsive core [12]. The value of the pairing gap averaged over the five single-particle states close to the Fermi energy [we take into account their degeneracy, i.e., $\Delta_F \equiv \sum_\nu (2j_\nu + 1)\Delta_{\nu\nu} / \sum_\nu (2j_\nu + 1)$, where the sum extends over $\nu = 3s_{1/2}, 2d_{5/2}, 2d_{3/2}, 1g_{7/2}$, and $1h_{11/2}$] is equal to $\Delta_F = 1.47$ MeV, which is close to the value derived from the experimental binding energies through the usual three-point formula. We also show by diamonds the values of $\Delta_{nnlj}$ obtained with the Argonne pairing interaction alone, corresponding to a value $\Delta_F = 1.04$ MeV. The state-dependent gaps obtained by solving the HFB equations including only the induced interaction are also shown by triangles in Fig. 3: The gap is concentrated close to the Fermi energy, and $\Delta_F = 1.11$ MeV. Negative values of the pairing gap associated with deep-lying levels are caused by the spin-dependent part of the induced interaction, associated with the Landau parameters $G_0$ and $G'_0$, which has a repulsive character, as discussed in Ref. [5]. This can be seen looking at Fig. 15(a) in Appendix B, where we report the same kind of calculations shown in Fig. 3, but including only the spin-independent part of the induced interaction (i.e., putting the Landau parameters $G_0$ and $G'_0$ equal to zero): In this case, the induced interaction alone leads to $\Delta_F = 1.88$ MeV, but adding the bare interaction [together with the $Z$ factor, cf. Eq. (5)] one obtains $\Delta_F = 2.12$ MeV. It is difficult to determine the spin-dependent part of the particle-hole interaction, and the balance between attraction and repulsion is rather dependent on the adopted parametrization. However,

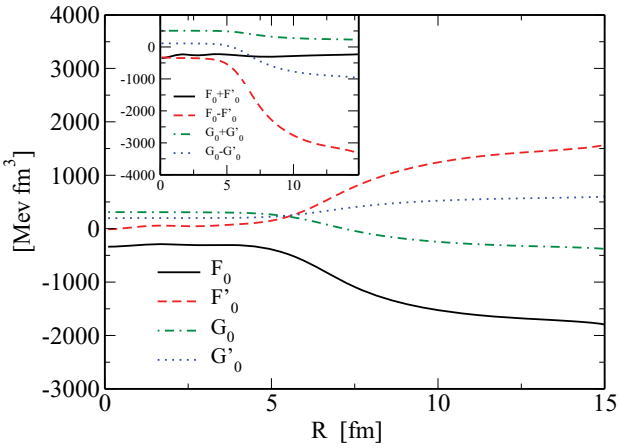


FIG. 2. (Color online) Landau-Migdal parameters associated with the SLy4 force, calculated as a function of the distance from the center of the nucleus in $^{120}$Sn.

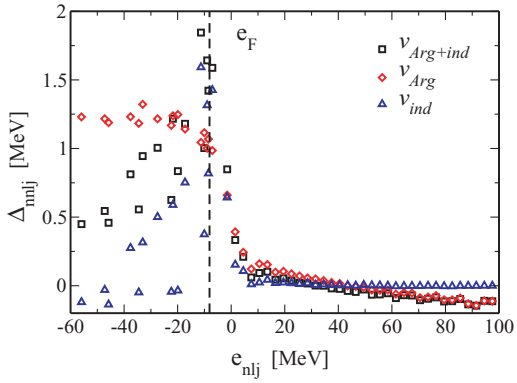


FIG. 3. (Color online) Diagonal matrix elements $\Delta_{nnlj}$ as a function of the single-particle energy $e_{nlj}$. The squares, diamonds, and triangles refer to the gaps obtained, respectively, with the Argonne plus induced interaction $v_{\text{Arg+ind}}$, with the Argonne interaction $v_{\text{Arg}}$, and with the induced interaction $v_{\text{ind}}$. The vertical dashed line indicates the position of the Fermi energy, which turns out to be almost the same for the three calculations.

the main factors determining the induced interaction in finite nuclei are the pronounced collective character of the surface modes and the dominance of the neutron-proton interaction over the neutron-neutron interaction: These determine its overall attractive character, in contrast with the case of uniform neutron matter [5]. Therefore, although the absolute value of the pairing gap could be somewhat different if we employed another interaction, we expect that the main trends of the spatial dependence discussed in the following would not be affected.

We also notice that the induced interaction is dominated by the contribution of isoscalar modes, whereas isovector modes reduce the gap slightly. Although $T$ is not a good quantum number, we have in fact found that by including only the modes that have a dominant $T = 0$ character the pairing gap produced by the induced interaction is increased from 1.11 to 1.30 MeV, whereas by including only modes with dominant $T = 1$ character we do not find any pairing gap.

For an interaction that depends only on the relative coordinate $r_{12}$, such as the Argonne interaction, the pairing field $\Delta(\vec{r}_1, \vec{r}_2)$ is directly related to the Cooper pair wave function introduced in Eqs. (2) and (3):

$$\Delta(\vec{r}_1, \vec{r}_2) = -v(r_{12})\Phi^{S=0}(\vec{r}_1, \vec{r}_2). \tag{13}$$

We note that the matrix elements of the induced interaction [cf. Eq. (6)] depend on the energies of the single-particle states through the energy denominators, and one cannot directly use Eq. (13) to obtain a corresponding pairing field. We shall instead use the fact that either one of the two bases $\psi_{nn'lj^\uparrow}$, with $j^\uparrow = |l + 1/2|, l = 0, 1, \ldots$, or $\psi_{nn'lj^\downarrow}$, with $j^\downarrow = |l - 1/2|, l = 0, 1, 2, \ldots$, is a complete basis in the $(J = 0, S = 0)$ subspace, constructing the associated pairing fields $\Delta^\uparrow$ and $\Delta^\downarrow$, as

$$\Delta^\uparrow(\vec{r}_1, \vec{r}_2) = \sum_{nn'lj^\uparrow} (2l + 1)\Delta_{nn'lj^\uparrow}\psi^{S=0}_{nn'lj^\uparrow}(\vec{r}_1, \vec{r}_2), \tag{14}$$

and similarly for $\Delta^\downarrow$, where the factor $(2l + 1)$ is a normalization factor associated with the Legendre polynomials. It turns out that there is some dependence on which basis is used. This is because of the structure of the denominators in Eq. (6) and the effect of the spin-orbit interaction. For simplicity, we shall limit ourselves in the following to the pairing field obtained by taking the average of the two expansions:

$$\Delta_{\rm ind} = \frac{\Delta^\uparrow + \Delta^\downarrow}{2}. \tag{15}$$

We shall show that this leads to a local expression for the pairing field, which reproduces rather well the quasiparticle energies and the pairing energies obtained by solving the original HFB equations [Eq. (1)].

We shall now study the Cooper wave function and the pairing field associated with the bare Argonne interaction and the pairing-induced interaction. In Fig. 4 we show the Cooper pair wave function $\Phi^{S=0}$ for fixed values of $R_{\rm c.m.}$ (the center of mass of the pair), as a function of the relative distance $r_{12}$. The wave function also depends weakly on the value of the angle $\theta_p$ between $\vec{R}_{\rm c.m.}$ and $\vec{r}_{12}$, and we show the result obtained after an angular average. At small values of the relative distance, $r_{12} < 1$ fm, the strong repulsive core

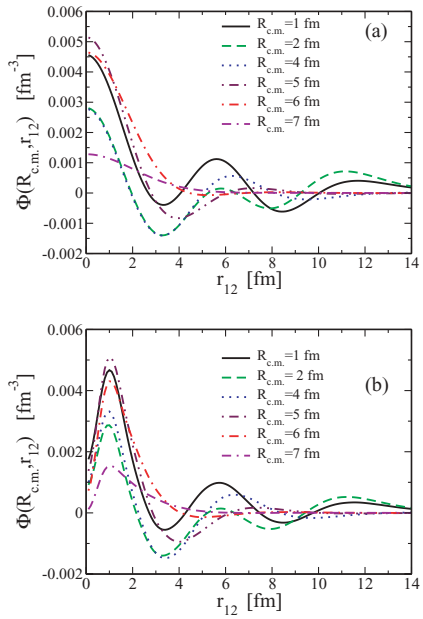


FIG. 4. (Color online) Abnormal density $\Phi(R_{\rm c.m.}, r_{12})$ for fixed values of $R_{\rm c.m.}$. In (a) we show the results calculated with the induced pairing interaction, in (b) those obtained with the Argonne pairing interaction.

present in the Argonne interaction prevents the two neutrons from staying close to each other, producing a hole in the wave function [see Fig. 4(b)]. For larger values of $r_{12}$ the wave functions are rather similar [see Figs. 4(a) and 4(b)], as can also be seen in Fig. 5, where we show the root-mean-square radius $\langle r_{12}^2\rangle^{1/2}$, as a function of the position of the center of mass [13]. In fact, $\Phi^{S=0}$ is dominated by the spatial dependence of the single-particle wave functions [14]. One can remark that, owing to the finite size of the nucleus, which limits the phase space available for the formation of Cooper pairs, the values of $\langle r_{12}^2\rangle^{1/2}$ are considerably smaller than the value of the coherence length $\xi$ in uniform neutron or nuclear matter at the corresponding density. In fact, $\xi$ can be estimated from $\xi = \hbar^2 k_F/m^*\pi\,\Delta_F$ [15,16], leading to $\xi \sim 19$ fm inside the nucleus

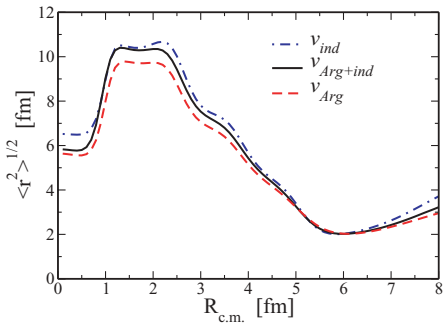


FIG. 5. (Color online) Root-mean-square radius of the Cooper pair as a function of the position of the center of mass, obtained with the Argonne+induced interaction $v_{\rm Arg+ind}$ (solid line), the Argonne interaction $v_{\rm Arg}$ (dashed line), and the induced interaction $v_{\rm ind}$ (dash-dotted line).

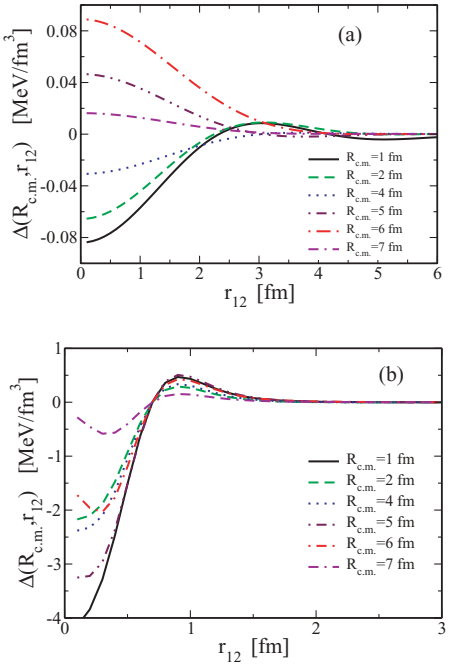


FIG. 6. (Color online) Pairing field $\Delta(R_{\text{c.m.}}, r_{12})$ for fixed values of $R_{\text{c.m.}}$. (a) Results calculated with the induced pairing interaction; (b) results obtained with the Argonne pairing interaction.

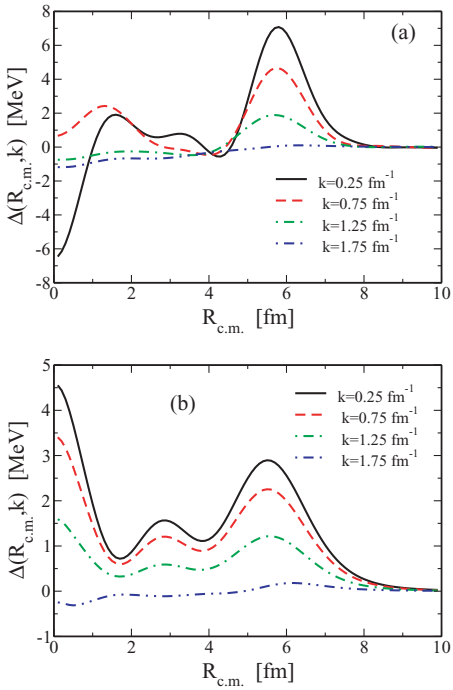


FIG. 7. (Color online) Pairing field [Eq. (16)] as a function of the position of the center of mass for different values of the relative momentum $k$, for (a) the Argonne plus induced interaction $v_{\text{Arg+ind}}$ and (b) the Argonne interaction $v_{\text{Arg}}$.

($m^* = 0.7\,m$, $k_F = 1.3$ fm$^{-1}$, $\Delta_F = 1$ MeV) and to $\xi \sim 6$ fm on the surface ($m^* = m$, $k_F = 0.9$ fm$^{-1}$, $\Delta_F = 2$ MeV).

In Fig. 6 we show the structure of the pairing field as a function of the relative distance for various values of the center-of-mass coordinate $R_{\text{c.m.}}$, averaged over the angle $\theta_p$. In the case of the Argonne interaction, the pairing field is obtained from Eq. (13), but in the case of the induced interaction it is obtained from Eq. (15), as previously discussed. The repulsive core produces the large negative quantities at small values of $r_{12}$ observed in Fig. 6(b), whereas the attractive part prevails for $r_{12} > 1$ fm. The induced gap [Fig. 6(a)] is strongly peaked around $R_{\text{c.m.}} \approx 6$ fm, in keeping with the fact that it receives the main contribution from the low-lying collective modes, whose transition density is concentrated on the surface of the nucleus [5,7]. The negative values for small $R_{\text{c.m.}}$ and $r_{12}$ in Fig. 6(a) are due to the repulsive, spin-dependent part of the interaction [cf. the corresponding Fig. 15(b) where this part has been left out]. We note the different energy scales in Figs. 6(a) and 6(b). In fact, the presence of the repulsive core in the bare interaction makes it difficult to assess the relevance of the induced interaction. It is more convenient to consider the dependence of the two interactions on relative momentum $k$, because the effect of the repulsive core is then restricted to high values of $k$, for which the induced interaction plays no role.

## III. MOMENTUM DEPENDENCE OF THE PAIRING FIELD AND ITS LOCAL APPROXIMATION

In this section we study the momentum dependence of the pairing field, by taking the Fourier transform of $\Delta(\vec{r}_1, \vec{r}_2)$ with respect to the relative distance $\vec{r}_{12}$:

$$\Delta(\vec{R}_{\text{c.m.}}, \vec{k}) = \int d^3 r_{12} e^{i\vec{k}\cdot\vec{r}_{12}} \Delta(\vec{R}_{\text{c.m.}}, \vec{r}_{12}). \tag{16}$$

We then average over the angle between $\vec{R}_{\text{c.m.}}$ and the relative momentum $\vec{k}$ and obtain a function $\Delta(R_{\text{c.m.}}, k)$ that depends only on the moduli of these two vectors. In Fig. 7 we plot $\Delta(R_{\text{c.m.}}, k)$ for $v_{\text{Arg}}$ and for the total interaction $v_{\text{Arg+ind}}$. For the bare interaction, the behavior at small values of $R_{\text{c.m.}}$ is dominated by the $3s_{1/2}$ orbit, whereas the negative values of $\Delta$ at high values of $k$ are due to the repulsive core [12]. Adding the induced interaction clearly has a strong effect on the pairing field for values of $k$ lower than about 1 fm$^{-1}$, enhancing the gap in the surface region and reducing it inside the volume of the nucleus.

One can obtain a local approximation to the pairing field, through a simple Thomas-Fermi approximation [16,17], by writing $\Delta_{\text{loc}}(R_{\text{c.m.}}) \equiv \Delta[R_{\text{c.m.}}, k_F(R_{\text{c.m.}})]$, where the local Fermi momentum is given by

$$\hbar^2 k_F^2(R_{\text{c.m.}}) = 2m^*(R_{\text{c.m.}})[e_F - U(R_{\text{c.m.}})], \tag{17}$$

where $U(R_{\text{c.m.}})$ is the HF potential and $m^*(R_{\text{c.m.}})$ is the effective mass [18] associated with the SLy4 interaction. Equation (17) is only valid in the classically allowed region where $e_F - U(R_{\text{c.m.}}) > 0$ (in the present case the turning point lies at $R_t = 7.1$ fm). We shall extend our definition into the classically forbidden region, using the Fourier transform at zero momentum:

$$\Delta_{\text{loc}}(R_{\text{c.m.}})_{\text{ext}} \equiv \Delta(R_{\text{c.m.}}, k = 0) = \int d^3 r_{12} \Delta(\vec{R}_{\text{c.m.}}, \vec{r}_{12}). \tag{18}$$

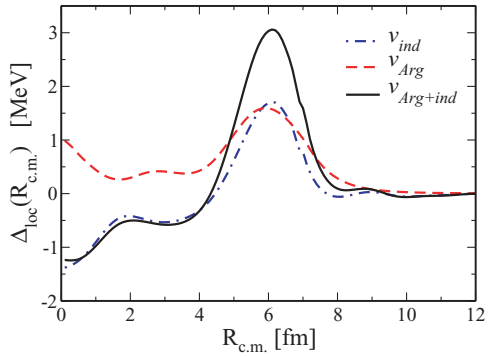


FIG. 8. (Color online) Pairing field obtained with the semiclassical approximation [cf. Eq. (19)] for the three different pairing interactions: Argonne plus induced $v_{\rm Arg+ind}$ (solid line), Argonne $v_{\rm Arg}$ (dashed line), and induced $v_{\rm ind}$ (dash-dotted line).

This is equivalent to using a local momentum associated with an energy slightly larger than $e_F$. In this way the pairing field

$$\Delta_{\rm loc}(R_{\rm c.m.}) = \begin{cases} \Delta[R_{\rm c.m.}, k_F(R_{\rm c.m.})], & R_{\rm c.m.} \leqslant R_t, \\ \Delta_{\rm loc}(R_{\rm c.m.})_{\rm ext}, & R_{\rm c.m.} > R_t, \end{cases} \tag{19}$$

is continuous, and we have found that the first derivatives also match to a good approximation. The resulting local pairing fields are plotted in Fig. 8. The pairing field associated with the Argonne interaction is rather surface peaked, going from 1.5 MeV at the surface to 0.5 MeV in the interior. Adding the induced interaction reinforces this surface character, leading to a large peak at the surface of about 3 MeV. The negative values of the gap in the interior of the nucleus are caused by the spin-dependent part of the induced interaction, as can be checked, by comparing with Fig. 15(f) in Appendix B, obtained by including only the spin-independent part of the interaction: In that case the pairing gap essentially vanishes inside the nuclear volume, whereas it reaches a value of about 4 MeV on the surface.

The local pairing field $\Delta_{\rm loc}(R_{\rm c.m.})$ can be used as the pairing potential in the HFB equations for a zero-range potential written in coordinate space [19]:

$$\left(\frac{d^2}{dR^2} - \frac{l(l+1)}{R^2} + \frac{2m^*}{\hbar^2}[e_F + E_{\rm qp} - U(R)]\right) u_{lj}(R) + \frac{2m^*}{\hbar^2}\frac{d}{dR}\left(\frac{\hbar^2}{2m^*}\right)\frac{d}{dR}u_{lj}(R) - \frac{2m^*}{\hbar^2}\Delta_{\rm loc}(R)v_{lj}(R) = 0,$$

$$\left(\frac{d^2}{dR^2} - \frac{l(l+1)}{R^2} + \frac{2m^*}{\hbar^2}[e_F - E_{\rm qp} - U(R)]\right) v_{lj}(R) + \frac{2m^*}{\hbar^2}\frac{d}{dR}\left(\frac{\hbar^2}{2m^*}\right)\frac{d}{dR}v_{lj}(R) + \frac{2m^*}{\hbar^2}\Delta_{\rm loc}(R)u_{lj}(R) = 0. \tag{20}$$

To test the reliability of the semiclassical $\Delta_{\rm loc}(R_{\rm c.m.})$ we have compared the quasiparticle energies and the occupation probabilities obtained by solving the self-consistent HFB equations [cf. Eq. (1)] using the full potentials, with the solution of Eq. (20) obtained using the local potential. The results are collected in Table I. The overall agreement is rather good: Most quasiparticle energies are reproduced within 200 keV and the occupation probabilities larger than 0.1 are reproduced within 15%. The local approximation introduced here, based on the results obtained in the microscopic HFB calculation, leads to pairing gaps that are rather different from those obtained from the simplest local density approximation (LDA), which does not take into account proximity effects associated with the nuclear surface and the fact that the nuclear radius is smaller than the coherence length in uniform matter. This can be seen in Fig. 9, where we compare the local pairing gap $\Delta_{\rm loc}$ associated with the Argonne interaction with the function $\Delta_{\rm LDA}(R_{\rm c.m.}) = \Delta_F^{\rm n.m.}[\rho_n(R_{\rm c.m.})]$, where $\Delta_F^{\rm n.m.}$ is the pairing gap calculated at the Fermi energy in uniform neutron matter, for a density equal to the neutron density at a distance $R_{\rm c.m.}$ from the center of the nucleus, using the local value of the effective mass. The LDA overestimates the difference between the pairing gap on the surface and in the interior of the nucleus, an effect already observed in the case of the inner crust in neutron stars [20].

## IV. LDA PARAMETRIZATION OF THE PAIRING INTERACTION

### A. Density-dependent, zero-range parametrization

The local pairing fields discussed in the previous section can be compared to those obtained by several authors, who

TABLE I. The lowest quasiparticle energies, expressed in MeV, associated with the quantum numbers $(l, 2j)$ obtained by solving the HFB equations [Eq. (1)] with the Argonne+induced, Argonne, and induced interactions are indicated with $E_{\rm qp}^{\rm full}$; also listed are the occupation probabilities $v_{\rm can}^2$ obtained in the canonical basis. They are compared with the quasiparticle energies $E_{\rm qp}^{\rm loc}$ and occupation probabilities $v_{\rm loc}^2$ (cf. Eq. (7) from Ref. [19]) obtained by solving the HFB equations [Eq. (20)] in coordinate space with the local pairing potentials shown in Fig. 8 and discussed in the text.

| $l$ $2j$ | $v_{\rm Arg+ind}$ | | | | $v_{\rm Arg}$ | | | | $v_{\rm ind}$ | | | |
|---|---|---|---|---|---|---|---|---|---|---|---|---|
| | $E_{\rm qp}^{\rm full}$ | $v_{\rm can}^2$ | $E_{\rm qp}^{\rm loc}$ | $v_{\rm loc}^2$ | $E_{\rm qp}^{\rm full}$ | $v_{\rm can}^2$ | $E_{\rm qp}^{\rm loc}$ | $v_{\rm loc}^2$ | $E_{\rm qp}^{\rm full}$ | $v_{\rm can}^2$ | $E_{\rm qp}^{\rm loc}$ | $v_{\rm loc}^2$ |
| 0 1 | 1.92 | 0.76 | 1.35 | 0.86 | 1.41 | 0.85 | 1.31 | 0.86 | 1.30 | 0.78 | 0.91 | 0.95 |
| 2 3 | 1.49 | 0.66 | 1.30 | 0.69 | 1.18 | 0.72 | 1.08 | 0.74 | 0.87 | 0.68 | 0.67 | 0.77 |
| 2 5 | 3.76 | 0.93 | 3.48 | 0.97 | 3.46 | 0.98 | 3.42 | 0.98 | 3.51 | 0.94 | 3.19 | 0.99 |
| 4 7 | 2.21 | 0.94 | 2.32 | 0.93 | 2.33 | 0.94 | 2.27 | 0.95 | 1.87 | 0.99 | 1.98 | 0.98 |
| 5 11 | 1.89 | 0.23 | 1.88 | 0.25 | 1.37 | 0.15 | 1.48 | 0.17 | 1.84 | 0.18 | 1.38 | 0.10 |

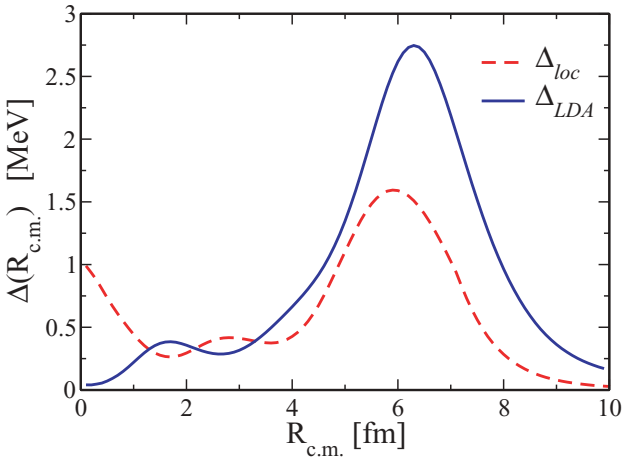


FIG. 9. (Color online) The local pairing gap calculated from Eq. (19) for the Argonne interaction, already shown in Fig. 8 (dashed line), compared to the gap obtained by using the simple LDA approximation (solid line).

employed a density-dependent pairing interaction (DDDI) of the form [21–24]

$$v^{\delta}(\vec{r}_1,\vec{r}_2) = v_0\left[1-\eta\left(\frac{\rho\left(\frac{\vec{r}_1+\vec{r}_2}{2}\right)}{\rho_0}\right)^{\alpha}\right]\delta(\vec{r}_1-\vec{r}_2), \quad (21)$$

where $\rho_0$ is the nuclear saturation density and $v_0$, $\eta$, and $\alpha$ are three parameters to be determined, together with the value of a cutoff energy in the single-particle energies $E_{\rm cut}$, needed to solve the HFB equations with a zero-range interaction [23,25]. The parameter $v_0$ together with $E_{\rm cut}$ defines the strength of the pairing interaction, whereas the other two parameters determine the shape of the pairing field. For a given value of $E_{\rm cut}$, the strength can be fixed at zero density to reproduce the neutron scattering length. We shall use the single-particle levels that lie up to 60 MeV above the Fermi energy,

TABLE II. Parameters of the DDDI, Eq. (21), producing pairing gaps that fit the local semiclassical pairing fields obtained with the Argonne and with the Argonne plus induced interaction. We compare the pairing gap at the Fermi energy and the pairing energies (in MeV) obtained with the full calculation, $\Delta_F^{\rm full}$ and $E_{\rm pair}^{\rm full}$, with the values obtained using the corresponding density-dependent interaction, $\Delta_F^{\delta}$ and $E_{\rm pair}^{\delta}$.

| Interaction | $\alpha$ | $\eta$ | $\Delta_F^{\rm full}$ | $\Delta_F^{\delta}$ | $E_{\rm pair}^{\rm full}$ | $E_{\rm pair}^{\delta}$ |
|---|---|---|---|---|---|---|
| $v_{\rm Arg}$ | 0.66 | 0.84 | 1.04 | 1.03 | −13.2 | −8.9 |
| $v_{\rm Arg+ind}$ | 2.0 | 1.32 | 1.47 | 1.28 | −15.78 | −14.47 |

following Ref. [24], and as a consequence we shall put $v_0 = -458.4$ MeV fm$^{-3}$.

The parameters $\alpha$ and $\eta$ have been determined in previous works to reproduce either experimental gaps or the pairing gap at the Fermi energy obtained with a finite range interaction such as Gogny or Argonne in uniform neutron matter. In this section we want instead to determine the parameters of the DDDI from the condition that the spatial dependence of the associated gaps reproduces that of the local pairing fields determined in the previous section [cf. Eq. (19)]. We solve the HFB equations [cf. Eq. (1)] for the pairing interaction [Eq. (21)]. We then fit the parameters $\eta$ and $\alpha$, minimizing the deviation between the form of the pairing gap obtained with the DDDI interaction of Eq. (21) and the form of the gap obtained with the local potentials. The values of the parameters for the various interactions are reported in Table II. Interestingly, the values we obtain for the Argonne interaction are very close to those obtained by Matsuo for the bare interaction in uniform neutron matter [24]. The values obtained for the Argonne+induced interaction correspond to a larger attraction in the surface region, in keeping with Fig. 8. The diagonal matrix elements of the pairing gap associated with $v_{\rm Arg}$ and $v_{\rm Arg+ind}$, already shown in Fig. 3, are compared with the corresponding quantities obtained by using the zero-range interaction in Fig. 10, where we also compare the spatial dependence of

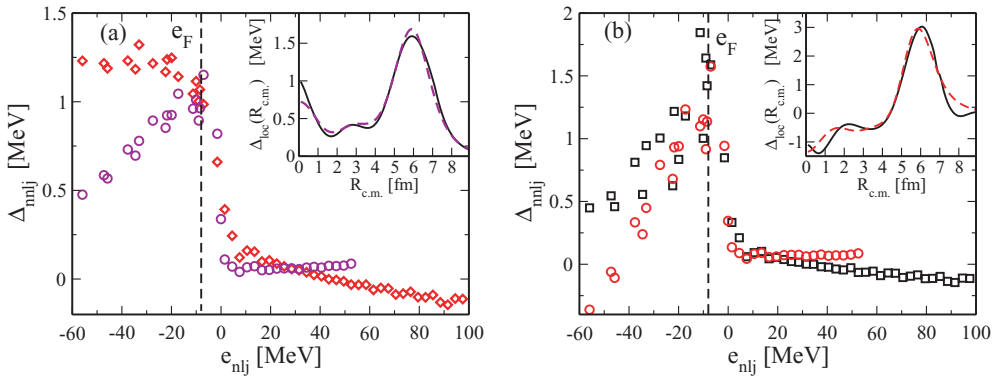


FIG. 10. (Color online) (a) The diagonal matrix elements of the pairing gap associated with the Argonne interaction $v_{\rm Arg}$ (diamonds, already shown in Fig. 3) compared with those associated with the DDDI, zero-range interaction with the parameters $\alpha = 0.66$, $\eta = 0.84$ (circles). The semiclassical pairing gaps associated with the Argonne interaction (solid line) and with the zero-range interaction (dashed line) are shown in the insert. (b) The diagonal matrix elements of the pairing gap associated with the Argonne+induced interaction $v_{\rm Arg+ind}$ (squares, already shown in Fig. 3) compared with the DDDI interaction with the parameters $\alpha = 2.0$, $\eta = 1.32$ (circles, cf. Table II). The semiclassical pairing gaps associated with the induced interaction (solid line) and with the zero-range interaction (dashed line) are shown in the insert.

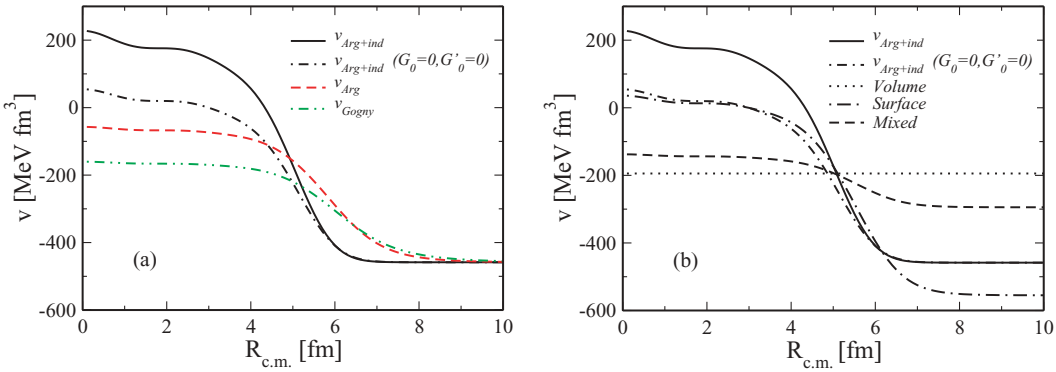


FIG. 11. (Color online) (a) Spatial dependence of the different local pairing interactions introduced in this work to simulate the local pairing gaps [cf. Eq. (19)] obtained with the corresponding microscopic, nonlocal interactions: bare+induced interaction $v_{\text{Arg+ind}}$ (corresponding to the parameters $\alpha = 2.0, \eta = 1.32$; cf. Table II); bare+induced interaction neglecting the spin-dependent part ($v_{\text{Arg+ind}}, G_0 = 0, G'_0 = 0$), ($\alpha = 1.79, \eta = 1.0$; cf. Table V in Appendix B); bare $v_{14}$ interaction $v_{\text{Arg}}(\alpha = 0.66, \eta = 0.84$; cf. Table II); Gogny interaction $v_{\text{Gogny}}$ ($\alpha = 0.51, \eta = 0.63$; cf. Table IV in Appendix A). (b) The spatial dependence of the bare+induced interaction with and without the spin-dependent part of the induced interaction, already shown in (a), compared with the volume, surface, and mixed interaction of Ref. [26] (see text).

the local pairing gaps (see insets). One can notice that the zero-range interaction (DDDI) yields a larger value of the gap for the levels above the Fermi energy. Nevertheless, we are able to reproduce the pairing energies associated with the Argonne+induced interaction within an accuracy of about 10% (cf. Table II). The agreement is not as good in the case of the pure Argonne interaction. In this case we could improve the agreement between the pairing energies by modifying the parameters slightly. We have found that using the parameters $\alpha = 0.7, \eta = 0.8$ we can reproduce the pairing energy within an accuracy of better than 5%, worsening somewhat the reproduction of the spatial dependence of the gap.

In Fig. 11(a) we compare the spatial dependence of the various local, density-dependent interactions, introduced here and also in Appendices A and B. The bare+induced interaction is considerably more attractive than the bare Argonne interaction or the effective Gogny interaction for $R_{\text{c.m.}} \sim 6$ fm. The effect of the spin-dependent part of the interaction, which produces a repulsive contribution in the nuclear interior, is also clearly seen in the figure. By construction, all the interactions tend to the value $v_0 = -458.4$ MeV fm$^{-3}$ for large values of $R_{\text{c.m.}}$. In Fig. 11(b) we compare our results for the bare+induced interactions (with and without the spin-dependent part) with the three schematic DDD interactions proposed in Ref. [26], where the associated pairing gaps have been compared with those extracted from the experimental odd-even mass differences. These interactions are of the form of Eq. (21) with $\alpha = 1$, and with $\eta = 0$ (volume force), $\eta = 1$ (surface force), and $\eta = 0.5$ (mixed force). The value of $v_0$ in this case has been obtained by imposing that the average value of the pairing field weighted with the nuclear density, $\bar{\Delta} \equiv \int d^3r \Delta(r)\rho(r)$, be equal to 1.24 MeV. (The cutoff adopted in Ref. [26] is slightly different from ours, and we have imposed the same condition within our space.) The definition of $\bar{\Delta}$ gives more weight to the value of the pairing field in the interior, compared to our definition of $\Delta_F$, which is based on the single-particle levels at the Fermi energy, which are more localized on the nuclear surface.

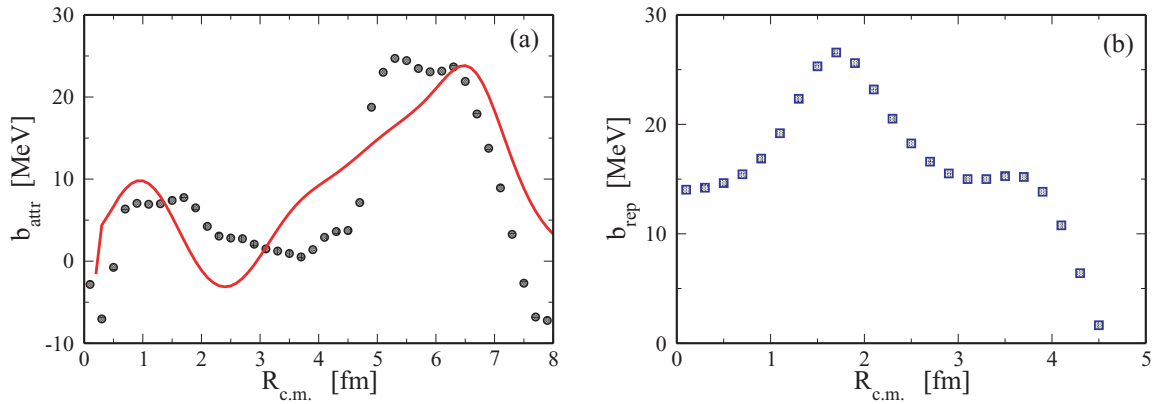


FIG. 12. (Color online) (a) The values of the parameter $b_{\text{attr}}$, obtained by fitting the Gaussian interaction [Eq. (23)], shown as a function of the center of mass $R_{\text{c.m.}}$ (filled dots) and compared with the function $0.14 R_{\text{nucl}} \frac{dU(r)}{dR_{\text{c.m.}}}$ (solid line). (b) The values of the parameter $b_{\text{rep}}$, obtained by fitting the Gaussian interaction [Eq. (23)], also shown as a function of the center of mass $R_{\text{c.m.}}$ (filled squares).

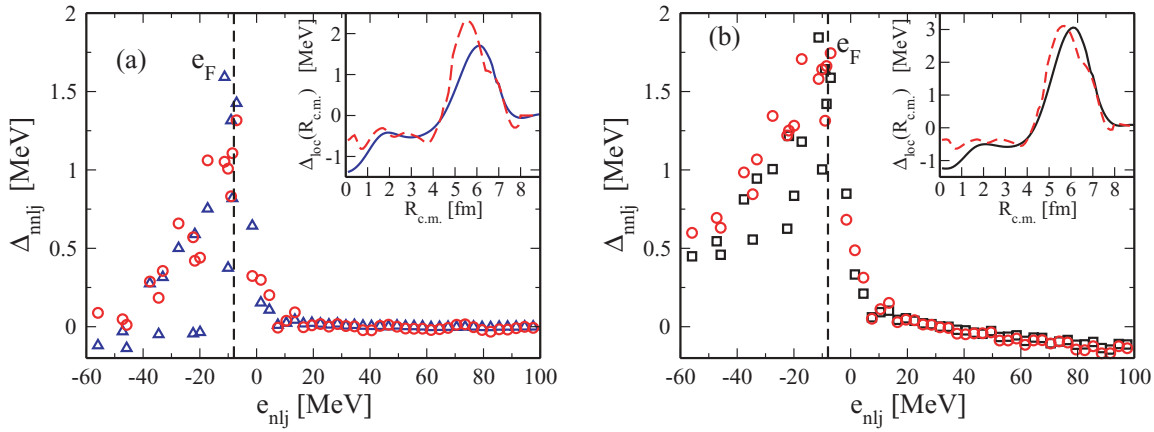


FIG. 13. (Color online) (a) The diagonal matrix elements of the pairing gap associated with the induced interaction $v_{\rm ind}$ (triangles, cf. Fig. 3) compared with those associated with the Gaussian parametrization [circles, cf. Eq. (23)]. The spatial dependence of the semiclassical pairing gap associated with the induced interaction (solid line) and with the Gaussian interaction (dashed line) are shown in the insert. (b) The same as (a), but for the Argonne+induced interaction $v_{\rm Arg+ind}$, shown by squares.

### B. Finite range parametrization

Within the zero-range parametrization just discussed, one can only try to fit the total bare+induced interaction, and since the resulting pairing interaction is a monotonic function of $R_{\rm c.m.}$, one cannot describe specific enhancements of the interaction localized on the nuclear surface or within the nuclear volume. We shall now discuss an alternative parametrization of $v_{\rm ind}$, based on the dominantly surface or volume character of the induced interaction associated, respectively, with the spin-independent or the spin-dependent part of the induced interaction.

We shall try to determine a Gaussian function $v^G_{\rm ind}(R_{\rm c.m.}, r_{12})$ to fulfill approximately the relation

$$\Delta(R_{\rm c.m.}, r_{12}) = -v^G_{\rm ind}(R_{\rm c.m.}, r_{12})\Phi^{S=0}(R_{\rm c.m.}, r_{12}). \quad (22)$$

We consider separately the contribution from the spin-independent, attractive and spin-dependent, repulsive parts of the interaction, writing $v^G_{\rm ind}(R_{\rm c.m.}, r_{12}) = v^G_{\rm attr}(R_{\rm c.m.}, r_{12}) + v^G_{\rm rep}(R_{\rm c.m.}, r_{12})$. We shall first fit the pairing gap obtained by including only the spin-independent part of $v_{\rm ind}$ and shown in Appendix B [cf. Fig. 15(b) and 15(c)], using the function

$$v^G_{\rm attr}(R_{\rm c.m.}, r_{12}) = -b_{\rm attr} \cdot \exp\{-[(r_{12} - c)/a_{\rm attr}]^2\}, \quad (23)$$

where $a_{\rm attr}$, $b_{\rm attr}$, and $c$ are parameters to be determined. We fix $c$ to constrain the Gaussian function to be maximum when at least one of the neutrons is on the surface of the nucleus. This implies $c = 2|R_{\rm nucl} - R_{\rm c.m.}|$, where $R_{\rm nucl} = 6.4$ fm is the location of the maximum of the first derivative of the single-particle potential. The parameter $a_{\rm attr}$ turns out in all cases to be very close to $a_{\rm attr} \approx 2$ fm, so in practice we have used a fixed value $a_{\rm attr} = 2$ fm. The resulting values of the parameter $b_{\rm attr}$ obtained as a function of $R_{\rm c.m.}$ are peaked on the nuclear surface and are plotted in Fig. 12(a). They can be rather well reproduced by the function $b_{\rm attr}(R_{\rm c.m.}) \sim \beta_{\rm ind} R_{\rm nucl} \cdot \frac{dU(R_{\rm c.m.})}{dR_{\rm c.m.}}$, where $\beta_{\rm ind} = 0.14$, which is of the order of the deformation parameter associated with the low-lying vibrational states.

The repulsive part of the induced interaction is active only in the interior of the nucleus, for $R_{\rm c.m.} \lesssim 4$ fm [cf. Fig 6(a) and Fig. 15(b) in Appendix B], so we multiply the Gaussian by a Heaviside function centered at $R_0 = 4.6$ fm:

$$v^G_{\rm rep}(R_{\rm c.m.}, r_{12}) = b_{\rm rep} \cdot \exp[-(r_{12}/a_{\rm rep})^2]\Theta(R_{\rm c.m.} - R_0). \quad (24)$$

We then determine the parameters of the repulsive Gaussian, fitting the values of $a_{\rm rep}$ and $b_{\rm rep}$ so that the resulting equation

$$v^G_{\rm ind}(R_{\rm c.m.}, r_{12}) = v^G_{\rm attr}(R_{\rm c.m.}, r_{12}) + v^G_{\rm rep}(R_{\rm c.m.}, r_{12}) \quad (25)$$

satisfies Eq. (22) for values of $r_{12}$ in the interval $[0, 2]$ fm, where we use in this case the gaps $\Delta(R_{\rm c.m.}, r_{12})$ and the Cooper pair wave function $\Phi^{S=0}(R_{\rm c.m.}, r_{12})$ obtained from the full calculation of the induced interaction considering both spin modes and density modes [see Figs. 4(a) and 6(a)]. The parameter $a_{\rm rep}$ turns out in all cases to be very close to $a_{\rm rep} \approx 3.5$ fm, so in practice we have used a fixed value $a_{\rm rep} = 3.5$ fm. The resulting values of $b_{\rm rep}$ are shown in Fig. 12(b) as a function of $R_{\rm c.m.}$.

In Fig. 13(a) we show the diagonal matrix elements of the pairing gaps and the semiclassical pairing gap obtained with the resulting Gaussian interaction, comparing it with the original induced interaction. In Fig. 13(b) we show instead the quantities obtained by adding the Argonne and the Gaussian interactions in analogy to Eq. (5). One can notice that the matrix elements $\Delta_{nnlj}$ are better reproduced with the Gaussian interaction than with the DDDI parametrization (cf. Fig. 9), leading to a better agreement with the value of $\Delta_F$ calculated with the full interaction (cf. Table III).

TABLE III. Average gaps and pairing energies (in MeV) obtained with the full calculation and with the Gaussian parametrization $v^G_{\rm ind}$.

| Interaction | $\Delta_F^{\rm full}$ | $\Delta_F^G$ | $E_{\rm pair}^{\rm full}$ | $E_{\rm pair}^G$ |
|---|---|---|---|---|
| $v_{\rm ind}$ | 1.11 | 1.13 | −7.41 | −7.99 |
| $v_{\rm Arg+ind}$ | 1.47 | 1.65 | −15.8 | −20.48 |

## V. CONCLUSIONS

The coupling of quasiparticles with collective surface vibrations gives rise to an induced pairing interaction that renormalizes the bare nucleon-nucleon interaction in an important way, leading to a total pairing field that is strongly peaked at the surface of the nucleus. Although the pairing-induced interaction is nonlocal and energy dependent, it is possible to adopt a semiclassical approximation, which yields a local pairing field that reproduces to good accuracy the features of the full quantal solution. This local field can also be obtained by adopting the widely used zero-range, density-dependent interaction, with an appropriate choice of the parameters, which turn out to be quite different from those usually employed in more phenomenological approaches. We have also given a simple and accurate finite range parametrization of the induced interaction.

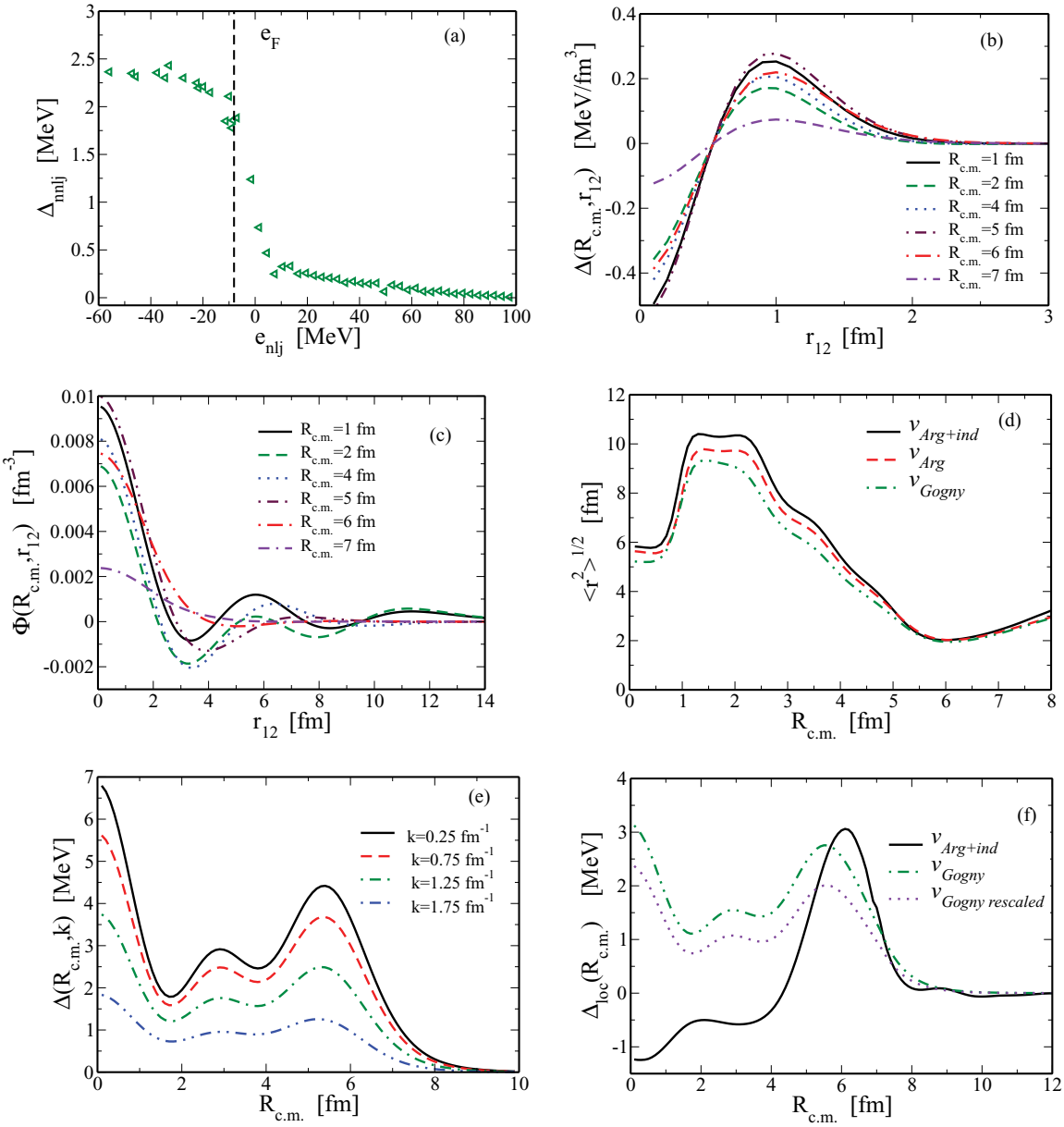


FIG. 14. (Color online) Different pairing gaps and Cooper pair wave functions obtained with the Gogny interaction. (a) Diagonal matrix elements $\Delta_{nnlj}$ as a function of the single-particle energy $e_{nlj}$. The vertical dashed line indicates the position of the Fermi energy. (b) Pairing gap $\Delta(R_{\text{c.m.}}, r_{12})$ in coordinate space for fixed values of $R_{\text{c.m.}}$. (c) Abnormal density $\Phi(R_{\text{c.m.}}, r_{12})$ in coordinate space for fixed values of $R_{\text{c.m.}}$. (d) Root-mean-square radius of the Cooper pair as a function of the position of the center of mass, for the Gogny interaction (dash-dotted curve), the Argonne interaction (dashed curve), and the Argonne+induced interaction (solid curve). (e) Pairing field [cf. Eq. (16)] as a function of the position of the center of mass for different values of the relative momentum $k$. (f) Pairing fields obtained with the semiclassical approximation [cf. Eq. (19)] for the Gogny interaction (dash-dotted curve) and for the Gogny interaction with rescaled matrix elements (dotted curve). They are compared with the pairing field associated with the Argonne+induced interaction (solid curve), already shown in Fig. 8.

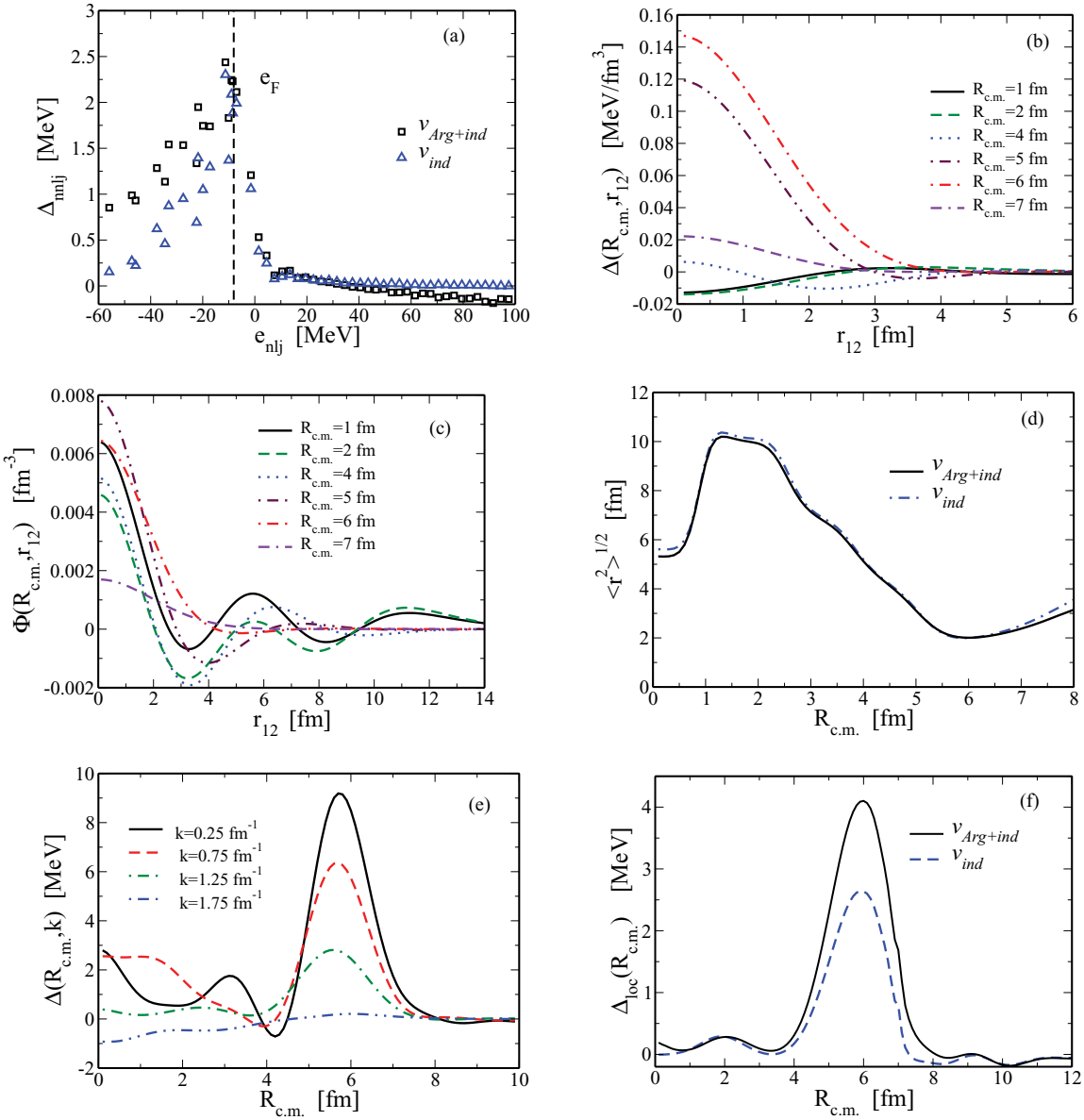


FIG. 15. (Color online) Different pairing gaps and Cooper pair wave functions obtained by including only the spin-independent part of the induced interaction. (a) Diagonal matrix elements $\Delta_{nnlj}$ as a function of the single-particle energy $e_{nlj}$. The vertical dashed line indicates the position of the Fermi energy. (b) Pairing gap $\Delta(R_{\rm c.m.}, r_{12})$ in coordinate space for fixed values of $R_{\rm c.m.}$. (c) Abnormal density $\Phi(R_{\rm c.m.}, r_{12})$ in coordinate space for fixed values of $R_{\rm c.m.}$. (d) Root-mean-square radius of the Cooper pair as a function of the position of the center of mass, for the induced interaction (dash-dotted curve) and the Argonne+induced interaction (solid curve). (e) Pairing field [cf. Eq. (16)] as a function of the position of the center of mass for different values of the relative momentum $k$. (f) Pairing fields obtained with the semiclassical approximation [cf. Eq. (19)] for the induced interaction (dashed curve) and for the Argonne+induced interaction (solid curve).


## ACKNOWLEDGMENTS

The authors thank S. Baroni for providing valuable help with QRPA calculations. F.B. acknowledges partial support from the Spanish Education and Science Ministry Project Nos. FPA2006-13807-c02-01, FIS2005-01105, and INFN08-33.


## APPENDIX A

In this Appendix, we investigate the properties of the Gogny D1S interaction. The Gogny interaction is an effective, finite range interaction that reproduces rather well the overall trends of the pairing gap along the mass table [27]. Compared to the bare force, it has a weak repulsive core and leads to larger gaps close to saturation density. In the following, we shall evaluate its properties in the pairing channel, starting from the same HF field obtained with the SLy4 interaction and previously used. The resulting properties, however, turn out to be similar to those obtained in a full HFB calculation with the Gogny force. This is because the values of the effective mass associated with the SLy4 and Gogny interactions are rather similar. In the specific case of $^{120}$Sn, the values of

TABLE IV. Parameters of the DDDI, Eq. (21), producing pairing gaps that fit the local semiclassical pairing fields obtained with the Gogny and with the rescaled Gogny interaction. We compare in the last two columns we compare the pairing gap at the Fermi energy and the pairing energy (in MeV) obtained with the full calculation, $\Delta_F^{\rm full}$ and $E_{\rm pair}^{\rm full}$, with the values obtained using the corresponding density-dependent interaction, $\Delta_F^{\delta}$ and $E_{\rm pair}^{\delta}$.

| Interaction | $\alpha$ | $\eta$ | $\Delta_F^{\rm full}$ | $\Delta_F^{\delta}$ | $E_{\rm pair}^{\rm full}$ | $E_{\rm pair}^{\delta}$ |
|---|---|---|---|---|---|---|
| $v_{\rm Gogny}$ | 0.51 | 0.63 | 1.92 | 2.05 | −20.4 | −26.6 |
| $v_{\rm Gogny}$, rescaled | 0.38 | 0.67 | 1.46 | 1.39 | −13.1 | −14.1 |

its matrix elements $\Delta_{nnlj}$, shown in Fig. 14(a), are close to 1.8 MeV, leading to an overestimate of the experimental gap.[1] The pairing gap $\Delta(R_{\rm c.m.}, r_{12})$ and the Cooper pair wave function $\Phi(R_{\rm c.m.}, r_{12})$ are shown in Figs. 14(b) and 14(c), and the root-mean-square radius of the Cooper pair is shown in Fig. 14(d). In Fig. 14(e) we show the Fourier transform of the pairing field. Finally, in Fig. 14(f) we show the semiclassical pairing gap $\Delta_{\rm loc}(R_{\rm c.m.})$. The volume part of the interaction is considerably more pronounced compared to the Argonne and to the Argonne+induced interaction.

To compare this semiclassical gap with the analogous quantities obtained for the Argonne+induced interaction presented in the main text, we also show the semiclassical field obtained after rescaling the matrix elements of the Gogny interaction by a factor 0.9, so as to obtain a value of the pairing gap of about 1.4 MeV at the Fermi energy. We also show in Table IV the parameters of the zero-range, density-dependent interaction obtained by fitting either the Gogny or the rescaled Gogny interaction.

[1] We note, however, that deducing the pairing gap from the calculated binding energy with the three-point formula would yield a better agreement.

TABLE V. Parameters of the DDDI [cf. Eq. (21)] producing pairing gaps that fit the local semiclassical pairing fields obtained with the Argonne plus the spin-independent part of the induced interaction. We compare the pairing gap at the Fermi energy and the pairing energy (in MeV) obtained with the full calculation, $\Delta_F^{\rm full}$ and $E_{\rm pair}^{\rm full}$, with the values obtained using the corresponding density-dependent interaction, $\Delta_F^{\delta}$ and $E_{\rm pair}^{\delta}$.

| Interaction | $\alpha$ | $\eta$ | $\Delta_F^{\rm full}$ | $\Delta_F^{\delta}$ | $E_{\rm pair}^{\rm full}$ | $E_{\rm pair}^{\delta}$ |
|---|---|---|---|---|---|---|
| $v_{\rm Arg+ind}$ | 1.79 | 1.0 | 2.12 | 2.17 | −26.6 | −31.4 |

## APPENDIX B

In this Appendix, we show the results obtained by neglecting the spin-dependent part of the induced interaction, that is, setting the Landau parameters $G_0, G_0'$ in Eq. (11) equal to zero. In this way one excludes the coupling with non-natural modes and produces a more attractive induced interaction. This can be seen, for example, by comparing the matrix elements of the pairing gap $\Delta_{nnlj}$ reported in Fig. 15(a), or the pairing gap in coordinate space reported in Fig. 15(b), with the corresponding results obtained with the full $v_{\rm ind}$ (cf. Fig. 3 and Fig. 6). The local pairing gap reaches a value of 4 MeV on the nuclear surface, to be compared with the value of 3 MeV with the full interaction [compare Fig. 15(f) and Fig. 8]. The Cooper pair wave function is much less sensitive to the features of the interaction, as we already noticed in the main text [compare Figs. 15(c) and 15(d) with Figs. 4 and 5]. We show in Table V the parameters of the zero-range, density-dependent interaction obtained by fitting the local pairing gap.


[1] D. M. Brink and R. A. Broglia, *Nuclear Superfluidity* (Cambridge University Press, Cambridge, England, 2005).
[2] F. Barranco, R. A. Broglia, G. Colò, G. Gori, E. Vigezzi, and P. F. Bortignon, Eur. Phys. J. A **21**, 57 (2004).
[3] F. Barranco, R. A. Broglia, G. Gori, E. Vigezzi, P. F. Bortignon, and J. Terasaki, Phys. Rev. Lett. **83**, 2147 (1999).
[4] J. Terasaki, F. Barranco, R. A. Broglia, E. Vigezzi, and P. F. Bortignon, Nucl. Phys. **697**, 127 (2002).
[5] G. Gori, F. Ramponi, F. Barranco, P. F. Bortignon, R. A. Broglia, G. Colò, and E. Vigezzi, Phys. Rev. C **72**, 011302(R) (2005).
[6] F. Barranco, P. F. Bortignon, R. A. Broglia, G. Colò, and E. Vigezzi, Eur. Phys. J. A **11**, 385 (2001).
[7] F. Barranco, P. F. Bortignon, R. A. Broglia, G. Colò, P. Schuck, E. Vigezzi, and X. Viñas, Phys. Rev. C **72**, 054314 (2005).
[8] G. Gori, F. Barranco, E. Vigezzi, and R. A. Broglia, Phys. Rev. C **69**, 041302(R) (2004).
[9] C. Mahaux, P. F. Bortignon, R. A. Broglia, and C. H. Dasso, Phys. Rep. **120**, 1 (1985).
[10] E. Chabanat, P. Bonche, and P. Haensel, Nucl. Phys. **A635**, 231 (1998).
[11] G. Colò and P. F. Bortignon, Nucl. Phys. **A696**, 427 (2001). Pairing correlations have been calculated in the BCS approximation with a simple seniority force, adjusted to the experimental pairing gap of $^{120}$Sn.
[12] M. Baldo, J. Cugnon, A. Lejeune, and U. Lombardo, Nucl. Phys. **A515**, 409 (1990).
[13] N. Pillet, N. Sandulescu, and P. Schuck, Phys. Rev. C **76**, 024310 (2007).
[14] N. Sandulescu, P. Schuck, and X. Viñas, Phys. Rev. C **71**, 054303 (2005).
[15] P. G. De Gennes, *Superconductivity of Metals and Alloys* (Addison-Wesley, Reading, MA, 1989).
[16] F. Barranco, R. A. Broglia, H. Esbensen, and E. Vigezzi, Phys. Rev. C **58**, 1257 (1998).
[17] P. Ring and P. Schuck, *The Nuclear Many-Body Problem* (Springer, New York, 2005).
[18] D. Vautherin and D. M. Brink, Phys. Rev. C **5**, 626 (1972).
[19] I. Hamamoto and B. R. Mottelson, Phys. Rev. C **68**, 034312 (2003).
[20] P. M. Pizzochero, F. Barranco, R. A. Broglia, and E. Vigezzi, Astrophys. J. **569**, 381 (2002).

[21] G. F. Bertsch and H. Esbensen, Ann. Phys. (NY) **209**, 327 (1991).
[22] E. Garrido, P. Sarriguren, E. Moya de Guerra, and P. Schuck, Phys. Rev. C **60**, 064312 (1999).
[23] A. Bulgac and Y. Yu, Phys. Rev. Lett. **88**, 042504 (2002).
[24] M. Matsuo, Phys. Rev. C **73**, 044309 (2006).
[25] P. J. Borycki, J. Dobaczewski, W. Nazarewicz, and M. V. Stoitsov, Phys. Rev. C **73**, 044319 (2006).
[26] J. Dobaczewski, W. Nazarewicz, and M. V. Stoitsov, in *Proceedings of the NATO Advanced Research Workshop on the Nuclear Many-Body Problem*, edited by W. Nazarewicz and D. Vretenar (Kluwer, Amsterdam, 2001), p. 181; J. Dobaczewski, W. Nazarewicz, and M. V. Stoitsov, Eur. Phys. J. A **15**, 21 (2002).
[27] S. Hilaire, J.-F. Berger, M. Girod, W. Satula, and P. Schuck, Phys. Lett. **B531**, 61 (2002).